Photocatalytic activity of CuO and Cu_2O nanowires

V. Scuderi[a*], G. Amiard[a], S. Boninelli[a], S. Scalese[b], M. Miritello[a], P. Sberna[b], G. Impellizzeri[a] and V. Privitera[a]

(a) CNR-IMM, Via S. Sofia 64, I-95123 Catania, Italy

(b) CNR-IMM, Z.I. VIII Strada 5, I-95121Catania, Italy

*Corresponding author: viviana.scuderi@imm.cnr.it

Keywords: CuO, Cu_2O, nanowires, photocatalytic activity, Methyl Orange.

http://dx.doi.org/10.1016/j.mssp.2015.08.008

Abstract

Here we report the photocatalytic efficiency of CuO and Cu_2O nanowires studied by dye degradation in water. The CuO nanowires were synthesized on Cu foils by thermal oxidation. A subsequent thermal annealing induced a controllable phase transformation of the nanowires and the underlying film from CuO to Cu_2O phase. A structural characterization was made by scanning and transmission electron microscopies, energy dispersive x-ray analysis and x-ray diffraction. The photocatalytic performances were evaluated by the degradation of two dyes in water: methylene blue and methyl orange. In particular, CuO nanowires showed a good photocatalytic activity in degrading methyl orange, compared with Cu_2O nanowires. The photocatalytic activity was correlated to the physical-chemical properties of the samples, revealing the detrimental effect of the polycrystalline structure for photocatalytic process.

1. Introduction

Cupric oxide (CuO) and cuprous oxide (Cu_2O) are P-type semiconductor with a narrow band gap of 1.2 eV and 2 eV, respectively. They received much attention for their numerous applications in several fields [1-4]. In particular, CuO has been extensively studied because of its close connection to high-*T*c superconductors [5], but it has also been widely exploited as a powerful

heterogeneous catalyst to completely convert hydrocarbons into carbon dioxide and water [6]. In addition, CuO and Cu_2O can be potentially used in gas sensors, solar cells, field emitters, electronic cathode materials and catalysts [2,3, 7-11].

Several methods were developed to synthesize CuO and Cu_2O with various morphologies, such as nanoparticles by alcohothermal decomposition of copper acetate [12], nanodendrite and microcrystals via the hydrothermal route [13,14], nanorods and nanoribbons by wet chemical methods [15]. The direct and simple thermal oxidation method was employed to synthesize CuO nanowires and nanorods. Many research teams prepared CuO nanowires successfully by oxidizing copper foils under different conditions of annealing temperatures, times and atmospheres [16,17].

Environmental safety has recently become one of the most serious concerns for the scientific community because of rapid increase of organic pollutants used in agriculture and various industries which cause severe adverse effects on the environment. Since photo-induced decomposition of water on TiO_2 electrodes was discovered [18], semiconductor-based photocatalysis has attracted extensive interest, in particular for water purification [19,20]. In this contest, CuO and Cu_2O are good promising candidates for wastewater treatment, because of their photocatalytic properties. However, due to the anisotropy of crystals, Cu_2O exhibits different stabilities, activities, etc. For example, octahedral Cu_2O with exposed {111} facets exhibited much higher photocatalytic activity than cubic Cu_2O [14].

In this work, we synthesized CuO nanowires by a thermal process in oxygen ambient of a Cu foil. Nanowires were morphologically and structurally characterized by scanning electron microscopy (SEM), transmission electron microscopy (TEM) and energy dispersive x-ray analysis (EDX). The material shows a high density of CuO nanowires, more than 10 μm in length and ~ 80 nm in mean diameter. A subsequent thermal annealing induced a controllable phase transformation of the nanowires and the underlying film from the CuO to Cu_2O. The photocatalytic activity of the synthesized nanowires were examined through the degradation of methyl blue and methyl orange,

in agreement with industry accepted international standards (ISO 10678:2010), and it was correlated to the physical-chemical properties of the materials.

2. Experimental methods

CuO nanowires were synthesized on Cu foils (purity of 99.9%, 0.4 mm thick) by thermal process in oxygen at the temperature of 550 °C for 3 h. Before of the thermal process, the copper foils were cleaned in acetone and isopropanol alcohol, under ultrasonic bath for 10 min, so to remove possible contaminations. After a drying process in air, the foils were annealed in a conventional furnace under a controlled O_2 flux.

The morphology and the chemical composition of the samples were investigated by field emission scanning electron microscopy (FE-SEM Zeiss Supra 35) operated at an acceleration voltage of 5 kV and equipped with energy dispersive X-ray spectroscopy (Aztec-EDS system by Oxford Instruments with 80mm^2 X-Max SDD detector).

The TEM characterization was made using a Jeol 2010F operated at 200 kV, in bright field and diffraction condition.

XRD measurements were acquired by Bruker D-500 difractometer at an angle of incidence of 0.8º, and Θ-2Θ from 20 to 60º. Acquired spectrum were analyzed by Bruker software suite, including ICSD structure database.

The photocatalytic activity of the investigated materials with respect to the degradation of organic compounds in water was evaluated by two colorants Methylene Blue (MB) and Methyl Orange (MO). The MB is a chemical compound commonly used to evaluate the photocatalytic efficiency of the materials, while MO is a toxic dye commonly used in the textile industry. A serious problem for the comparison of experimental results from different laboratories is the fact that every research group is still using its “own” chemical test system for the evaluation of the photocatalytic activities. In this work we use an experimental setup in agreement with the

international standards ISO 10678:2010. This protocol requires, like light source, a lamp in the range of 320-400 nm. The samples, 1 cm^2 in size, were immersed in a solution (2 ml) containing MB or MO and de-ionized water (starting concentration: 1.5×10^{-5} M and 1×10^{-5} M, respectively). The mixture was irradiated by an UV lamp (350-400 nm wavelength range) with a power of 8 W for 4 hours. Every 30 minutes, for the first two hours (and then every hour), of irradiation the solution was measured with a UV-VIS spectrophotometer (Perkin-Elmer Lambda 45) in a wavelength range between 500-800 nm for MB and 350-650 nm for MO. The degradation of MB and MO was evaluated by the absorbance of the peak at 664 nm and 464 nm respectively, thanks to the Lambert-Beer law ($A = \varepsilon \times l \times C$, where A is the absorbance of the solution at 664 or 464 nm, ε is the extinction molar coefficient, l is the width of the cuvette, C is the concentration of the MB or the MO) [21]. The decomposition of the colorants in absence of catalyst materials was also checked as a reference. Before the measurements, the samples were irradiated by the UV lamp for 50 min in order to remove the possible presence of hydrocarbons on the sample surface [22].

3. Results and discussion

Figure 1 (a) reports SEM images of nanowires (NWs) grown with high density by oxidation of a Cu sheet for 3 h at 550°C. The growth of the nanowires was preceded by a deformation of the substrate due to a straining force, with the formation of a hill and valley structure, in accordance with the literature [23]. SEM analyses in cross-view (not reported here) allowed to determine a mean length of the NWs of 10 μm and a mean diameter of ~ 80 nm. Figure 1(b) reports the SEM image of the NWs after a subsequent thermal annealing in vacuum for 3 h at 400 °C. They appear bent compared to the as-grown NWs.

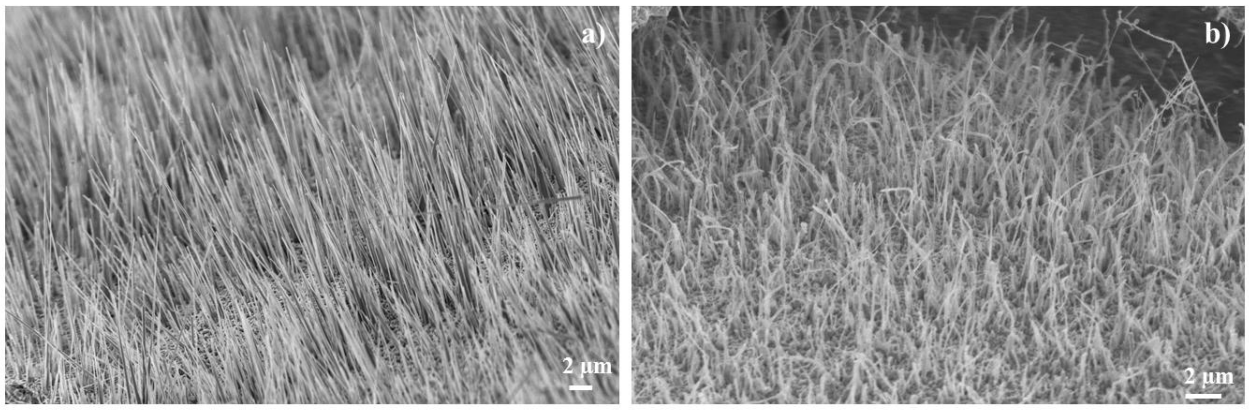

Fig. 1: Plan view SEM images of nanowires growth on copper foil: (a) by thermal process in oxygen at 550°C for 3h, (b) after a thermal annealing in vacuum at 400°C for 3h.

The chemical composition was investigated by XRD and EDX analysis. In particular, Figure 2 shows the XRD spectra of the NW before and after a subsequent thermal treatment in vacuum at 400 °C for 3 h. The mixture phase of CuO and Cu_2O can be detected in both samples. In more detail, before of the annealing (dotted line in Fig. 2) CuO is the prevailing phase (indicated with "A" in the figure), after the annealing (continuous line) the prevailing phase is Cu_2O (indicated with "B" in the figure). The signals indicated with the asterisks came from the substrate (Cu foil).

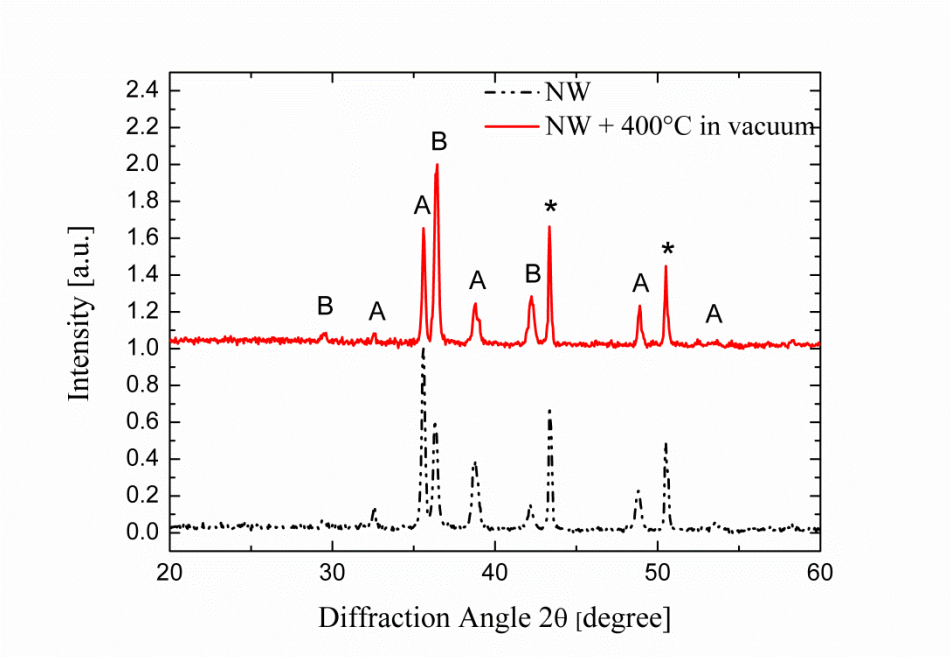

Fig. 2: XRD patterns of the NWs before (dotted line) and after the annealing (continuous line). "A" refers to CuO phase, "B" refers to Cu_2O phase, "*" refers to Cu.

Figure 3 reports the EDX spectra collected by SEM in cross-section, on the surface of the nanowires before (Fig. 3 (a)) and after (Fig. 3 (b)) the thermal treatment in vacuum. Only the presence of Cu and O is detected, in addition to adventitious carbon. In the inset of the EDX spectra, we report the tables of the detected elements with the relative percentage in weight (Wt%). From these percentages was possible to determine the stoichiometry of NWs by the equation:

$$\%_x = PM_x \times 100 / PM_{compound} \quad (1)$$

where $\%_x$ is the relative percentage in weight of the x element; PM_x is the molecular weight of the x element: $PM_{compound}$ is the molecular weight of the compound. Adventitious carbon is not considered in the calculation. In particular, the as-grown NWs are composed of CuO. After the thermal treatment in vacuum, the chemical composition changes and it is moves to Cu_2O phase.

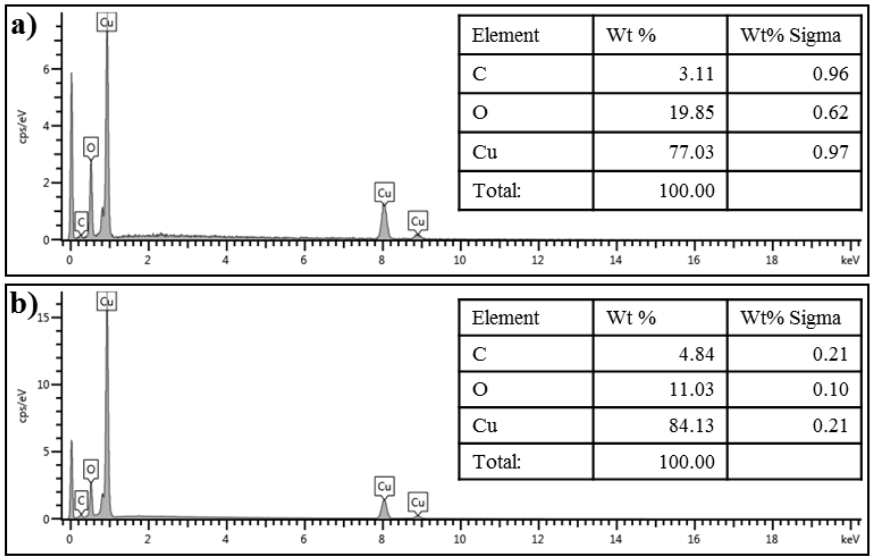

Element	Wt %	Wt% Sigma
C	3.11	0.96
O	19.85	0.62
Cu	77.03	0.97
Total:	100.00	

Element	Wt %	Wt% Sigma
C	4.84	0.21
O	11.03	0.10
Cu	84.13	0.21
Total:	100.00	

Fig. 3: EDX spectra with the tables of the detected elements, for: (a) nanowires growth by thermal process in oxygen at 550°C for 3h, and (b) after a thermal annealing in vacuum at 400°C for 3h.

Figure 4 reports TEM images of CuO (Fig. 4 (a)) and Cu_2O nanowires (Fig. 4 (b)). The TEM characterization shows the mono-crystalline structure of CuO-NWs, detecting few defects. It was confirmed by a diffraction analysis on a selected area, as reported in the inset of Fig. 4 (a). We can observe a 111 orientation of the CuO mono-crystal which was confirm by Carine simulation.

Instead, Cu_2O-NWs appeared poly-crystalline, as confirmed by the diffraction (inset Fig. 4(b)) and dark-field characterizations (not reported here).

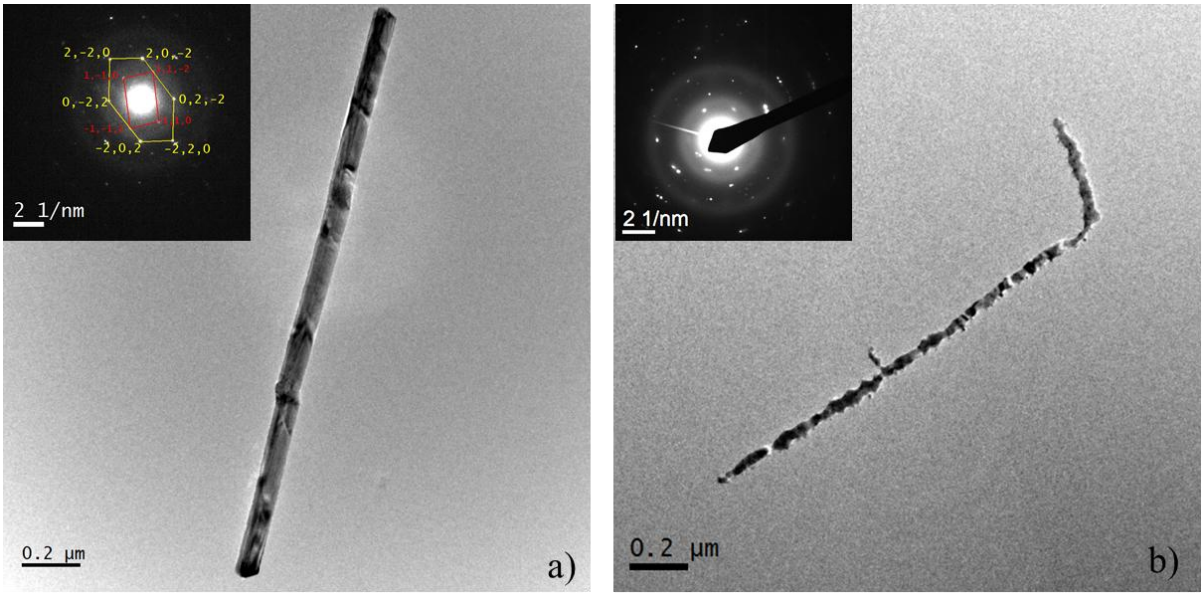

Fig. 4: TEM analysis of: (a) mono-crystalline CuO nanowires, (b) poly-crystalline Cu_2O nanowires. The diffraction patterns are reported in the insets.

The ability of the synthesized material in degrading organic pollutants was tested with MB and with MO. Methyl orange, is a toxic dye compound commonly used in textile, leather tanning and paper production industries. In detail, azo dyes represent about 50-70% of the waste dyes produced by the industries [24], and about 10-15% of them comes from the textile industry [25]. CuO and Cu_2O nanowires did not show a significant efficiency in degrading the MB (the results are not reported here). This depends on the nature of the MB and NWs: MB is a cationic dye, and CuO and Cu_2O are a P-type semiconductor [26,2]. Therefore, the absorption of the compound on the surface of the nanostructures is hindered because of the electrostatic repulsions between the positive molecular charge of the MB and the P-type semiconductor. This confirms that the nature of the organic compound and the nanostructures is fundamental in the first step of a photocatalytic process, that is the adsorption. This is not the case of MO, since it is an anionic dye.

Figure 5 reports the logarithmic residual concentration of MO under UV light, versus the irradiation time. In particular, C is the concentration of the MO after the irradiation, C_0 is the starting concentration of the MO.

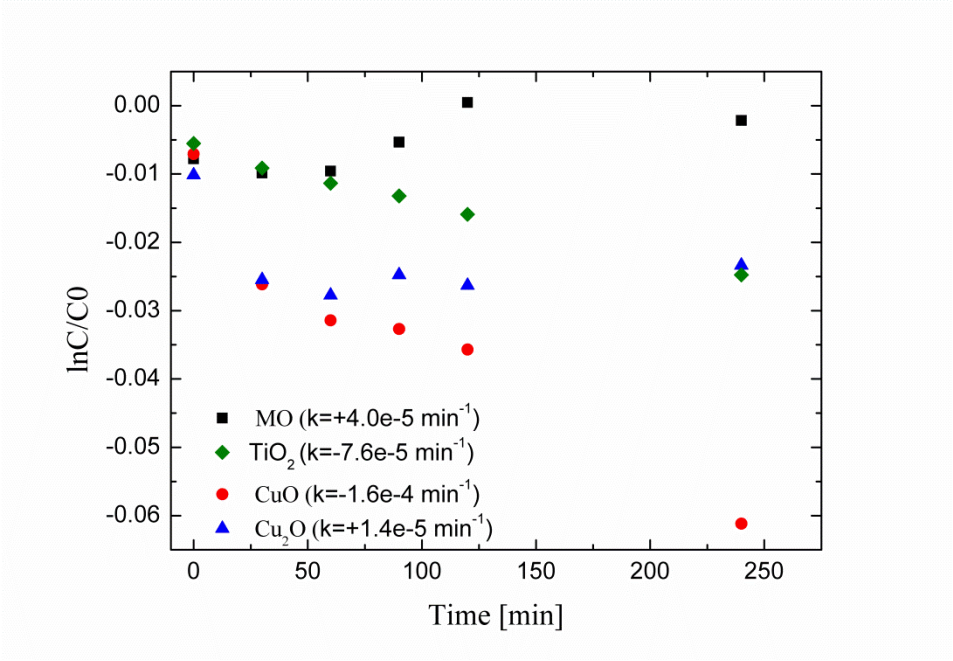

Fig. 5: MO degradation under UV light for three samples: MO (squares), MO with tiO2 thin film (diamond), MO with CuO-NW (circles), MO with Cu_2O-NW (triangles).

We tested four samples: MO in absence of any catalyst materials (squares), MO with TiO_2 thin film (diamond), MO with CuO-NWs (circles), MO with Cu_2O-NWs (triangles). TiO_2 film was deposited on Si substrate, with a Picosun R-200 advanced system. The film thickness (~10 nm) was evaluated by the M-2000 spectroscopic ellipsometer by Woollam. This film was used as reference sample.

Preconditioning process was applied to remove possible adsorbed organic pollutants on the surfaces [see the Experimental Method section]. The samples were immersed in the MO solutions and kept in the dark more than one hour. This process allows evaluating the absorption of the MO on the different sample surfaces without involving any photocatalytic reaction. However nanowires do not show absorption. After this step, the samples were exposed to the UV light, so to induce the photocatalysis. The observed reaction rate, k, follows a Lagmuir-Hinshelwood model kinetics, which can be expressed by a first-order reaction kinetic:

$$\ln\left(\frac{C}{C_0}\right) = -kt$$

where C is the concentration of organic species, C_0 is the initial concentration of organic species, t is the irradiation time [27]. The values are reported in Figure 5 for all the analyzed samples. For MO and Cu_2O-NWs, k has a positive value, due to the evaporation of the solvent content in MO solution and due to the incapability of the Cu_2O-NWs in degrading the MO. Consequently, there is an increase of the MO concentration in the solutions increasing the exposition time. While for TiO_2 thin film and CuO-NWs, the k value is negative, due to the ability of the samples in degrading MO. In particular, CuO-NWs shows the best photocatalytic activity.

It is reported in literature that the reaction rate, k, depends linearly on the amount of the photocatalytic material present in the solution [28]. However, it is difficult to make a comparison with the reaction rate values reported in the literature, because of the wide range of experimental conditions used, such as: power lamp, spectral range, dye concentration, presence of hydrogen peroxide in solution to increase the photocatalytic ability of the material [29,30].

In comparison with TiO_2 thin film, Cu+ promoted electron-hole generation due to the lower band gap, and the existence of copper is beneficial in transferring photo induced electrons and enhancing the separation efficiency of photo-induced electron hole pairs, which can reduce the rate of charge-carrier recombination. Consequently, the rate of the primary interfacial charge transfer increases [31]. The different response of CuO and Cu_2O nanowires in the degradation of MO probably depends on the different structure of the wires: mono-crystalline for CuO and poly-crystalline for Cu_2O-NWs (as revealed by diffraction analyses). In addition, the transformation of the nanowires and the underlying film from the CuO to Cu_2O phase introduces many defects in the structure, as revealed by the TEM analyses (Fig. 3(b)). It is well known that defects in TiO_2 play a crucial role in the photocatalyitc properties of the titanium dioxide. In particular, the nature of defects is fundamental because they can on one hand increase the photocatalyitc efficiency (i.e. oxygen vacancies) [32] or, on the other hand, they can act as recombination centers for electrons

193 and holes [33]. Moreover, poly-crystalline Cu_2O-NWs expose different facets, that have different
194 photocatalytic activity [34].
195

196 **4. Conclusion**

197 In this work, we synthesized CuO nanowires by a simple thermal process of Cu foils in a
198 controlled oxygen ambient. XRD, EDX and TEM analysis confirmed that a subsequent thermal
199 treatment in vacuum is able to modify the chemical structure of the nanowires and of the underlying
200 film from CuO to Cu_2O. The synthesized CuO-NWs revealed a photocatalytic activity in the
201 degradation of methyl orange higher than the one of Cu_2O-NWs. The different response probably
202 depends on the large amount of defects induced by the thermal treatment in vacuum due to the
203 formation of a polycrystalline structures. The importance to study and obtain high aspect-ratio
204 nanostructures and, in future, to join the investigated material with different semiconductors should
205 be evaluated to try to increase the photocatalytic efficiency in degrading organic pollutants.
206

207 **Acknowledgments**

208 This research has been supported by the FP7 European Project WATER (Grant Agreement
209 316082). Authors are grateful to L. Romano (University of Catania) for useful discussions.
210

211 **References**

212 [1] A.E. Rakhshani, Solid-State Electron. 29 (1986) 7-17.

213 [2] A.O. Musa, T. Akomolafe, M. Carter, J. Sol. Energy Mater. Sol. Cells 51 (1998) 305.

214 [3] J.T. Zhang, J.F. Liu, Q. Peng, X. Wang, Y.D. Li, Chem. Mater. 18 (2006) 867.

215 [4] P. Poizot, S. Laruelle, S. Grugeon, L. Dupront, J.M. Tarascon, Nature 407 (2000) 496-499.

[5] M.K. Wu, J.R. Ashburn, C.J. Torng, P.H. Hor, R.L. Meng, L. Gao, Z.J. Huang, Y.Q. Wang, C.W. Chu, Phys. ReV. Lett. 58 (1987) 908-910.

[6] J.B. Reitz, E.I. Solomon, J. Am. Chem. Soc. 120 (1998) 11467-11478.

[7] A. Chowdhuri, P. Sharma, V. Gupta, K. Sreenivas, K.V. Rao, J. Appl. Phys. 92 (2002) 2172-2180.

[8] S. Ghosh, D.K. Avasthi, P. Shah, V. Ganesan, A. Gupta, D. Sarangi, R. Bhattacharya, W. Assmann, Vacuum 57 (2000) 377-385.

[9] C.T. Hsieh, J.M. Chen, H.H. Lin, H.C. Shih, Appl. Phys. Lett. 83 (2003) 3383.

[10] S. Anandan, X. Wen, S. Yang, Mater. Chem. Phys. 93 (2005) 35-40.

[11] S. Bennici, A. Gervasini, Appl. Catal. B 62 (2006) 336-344.

[12] Z.S. Hong, Y. Cao, J.F. Deng, Mater. Lett. 52 (2002) 34-38.

[13] S. Li, H. Zhang, Y. Ji, D. Yang, Nanotechnology 15 (2004) 1428.

[14] Z. Zheng, B. Huang, Z. Wang, M. Guo, X. Qin, X. Zhang, P. Wang, Y. Dai. J. Phys. Chem. C 2009, 113, 14448–14453.

[15] Y. Chang, H.C. Zeng, Cryst. Growth Des. 4 (2004) 397-402.

[16] X. Jiang, T. Herricks, Y. Xia, Nano. Lett. 2 (2002) 1333-1338.

[17] M. Kaur, K.P. Muthe, S.K. Despande, S. Choudhury, J.B. Singh, N. Verma, S.K. Gupta, J.V. Yakhmi, J. Crystal Growth 289 (2006) 670-675.

[18] A. Fujishima, K. Honda, Nature 238 (1972) 37-38.

[19] C.W.K. Chow, C. Saint, Water Res. 44 (2010) 2997-3027.

[20] V. Scuderi, G. Impellizzeri, L. Romano, M. Scuderi, M.V. Brundo, K. Bergum, M. Zimbone, R. Sanz, M.A. Buccheri, F. Simone, G. Nicotra, B.G. Svensson, M.G. Grimaldi, V. Privitera, Nanoscale 6 (2014) 11189- 11195.

[21] McNaught A D and Wilkinson A 1997 Compendium of Chemical Terminology, 2nd ed. (the "Gold Book"). Blackwell Scientific Publications, Oxford.

[22] R. Wang, K. Hashimoto, A. Fujishima, M. Chikuni, E. Kojima, A. Kitamura, M. Shimohigoshi and T. Watanabe, Nature 388 (1997) 431-432.

[23] M. Kaur, K.P. Muthe, S.K. Despande, Shipra Choudhury, J.B. Singh, Neetika Verma, S.K. Gupta, J.V. Yakhmi, Journal of Crystal Growth 289 (2006) 670–675.

[24] R. Nilsson, R. Nordlinder, U. Wass, British J. Ind. Medical 50 (1993) 65-70.

[25] H. Zollinger (Ed.), Color Chemistry 1991 Synthesis, Properties and Applications of Organic Dyes and Pigments, 2nd Revised Edition VCH.

[26] H. Park, W. Choi, J. Phys. Chem. B 109 (2005) 11667–11674.

[27] M.N. Chong, B. Jin, C.W.K. Chow, C. Saint, Water Res. 44 (2010) 2997- 3027.

[28] M. Zimbone, M.A. Buccheri, G. Cacciato, R. Sanz, G. Rappazzo, S. Boninelli, R. Reitano, L. Romano, V. Privitera, M.G. Grimaldi. Applied Catalysis B: Environmental 165 (2015) 487–494.

[29] X. Liu, Z. Li, Q. Zhang, F. Li, T. Kong. Materials Letters 72 (2012) 49–52.;

[30] S. Zaman, A. Zainelabdin, G. Amin, O. Nur, M. Willander. Journal of Physics and Chemistry of Solids 73 (2012) 1320–1325.

[31]C. Dong, M. Zhong, T. Huang, M. Ma, D. Wortmann, M. Brajdic, I. Kelbassa, ACS Appl. Mater. Interfaces 3 (2011) 4332–4338

[32] A. Fujishima, X. Zhangb, D.A. Tryk, Surface Science Reports 2008, 63, 515- 582.

[33] G. Impellizzeri, V. Scuderi, L. Romano, P.M. Sberna, E. Arcadipane, R. Sanz, M. Scuderi, G. Nicotra, M. Bayle, R. Carles, F. Simone, V. Privitera, J. Appl. Phys. 116 (2014) 173507-8.

[34] Z. Zheng, B. Huang, Z. Wang, M. Guo, X. Qin, X. Zhang, P. Wang, Y. Dai. J. Phys. Chem. C 2009, 113, 14448–14453.

Figure
Click here to download high resolution image

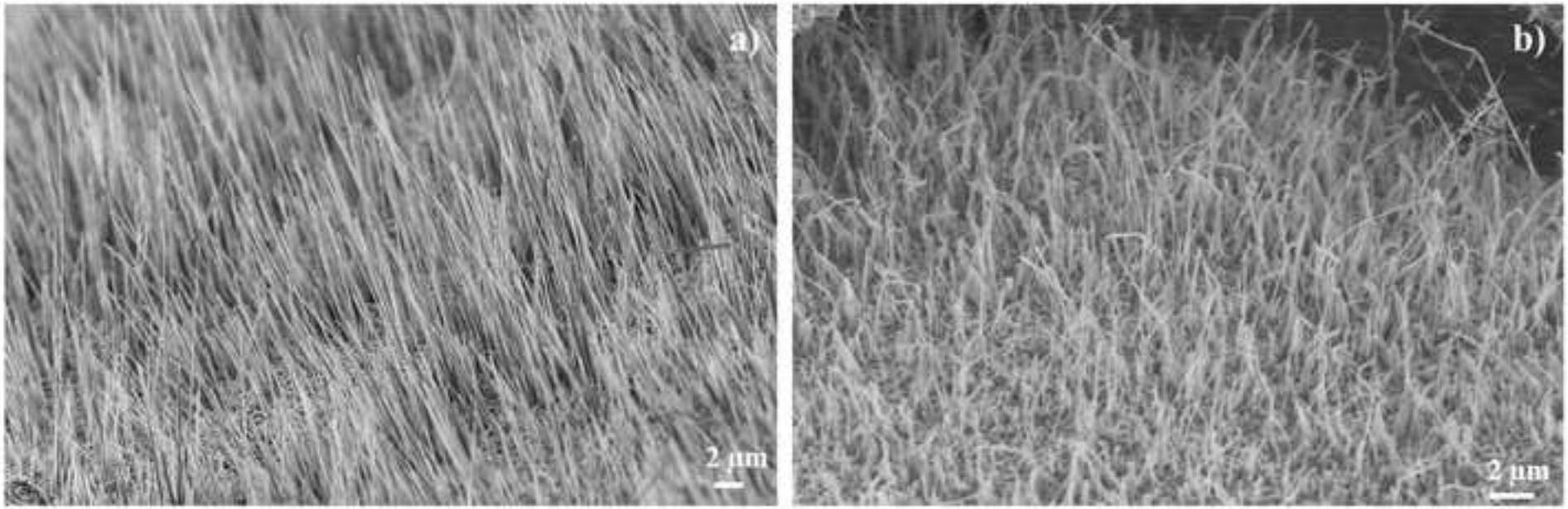

Figure
Click here to download high resolution image

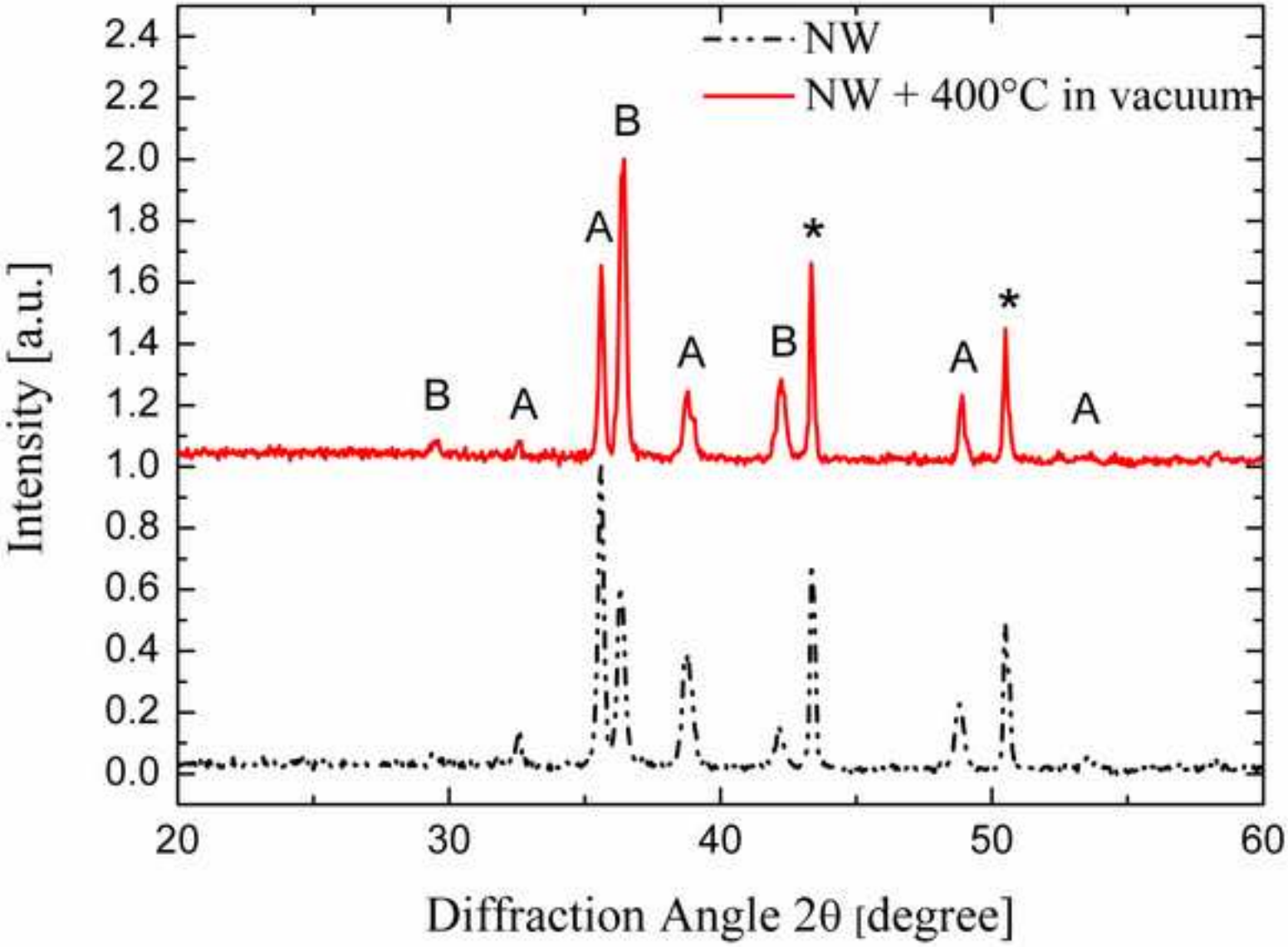

Figure

Click here to download high resolution image

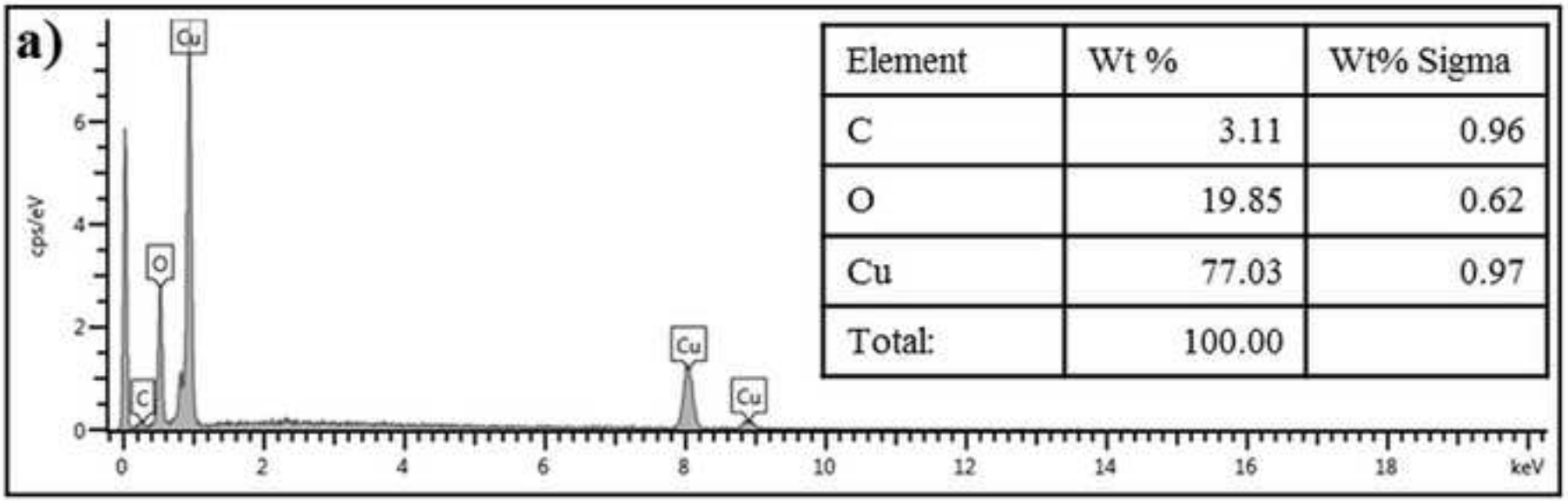

Element	Wt %	Wt% Sigma
C	3.11	0.96
O	19.85	0.62
Cu	77.03	0.97
Total:	100.00	

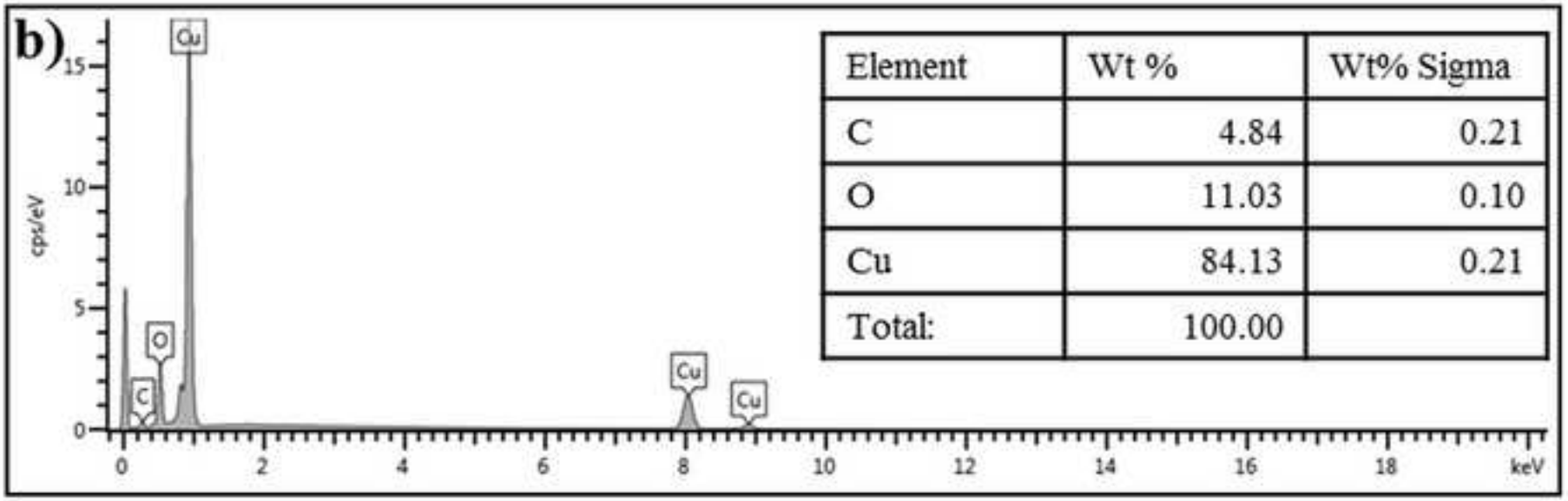

Element	Wt %	Wt% Sigma
C	4.84	0.21
O	11.03	0.10
Cu	84.13	0.21
Total:	100.00	

Figure

Click here to download high resolution image